Robustness Examinations on shipborne GNSS-IR wave gauge

李, 広聚
九州大学大学院総合理工学府総合理工学専攻地球環境理工学メジャー

令和７年度

九州大学大学院総合理工学府

総合理工学専攻地球環境理工学メジャー修士論文

Robustness Examinations on shipborne GNSS-IR wave gauge

氏　　名 李広聚　　(Guangju Li)

指導教員名 市川　香 (Kaoru Ichikawa)

Robustness Examinations on shipborne GNSS-IR wave gauge

Abstract: Shipborne Global Navigation Satellite System interferometric reflectometry (GNSS-IR) has recently been proposed as a low-cost wave-gauge technique for estimating significant wave height (SWH) and wave period from operating vessels. Although the feasibility of this approach was demonstrated by Ichikawa et al. (2024), their validation relied on only 3 representative cases, leaving the robustness and statistical reliability of the method insufficiently assessed. The primary objective of this study is therefore to evaluate the robustness of the existing shipborne GNSS-IR wave-gauge framework with more than 90 cases. Availability of low-elevation satellites, which are necessary for GNSS-IR, is found not always satisfied with the present sensor settings. In addition, the estimated SWH is found underestimated, especially when the sea state is rougher. This suggests that GNSS-IR wave gauge has a limitation for applying rough sea states.

Keywords: ship-borne; significant wave height; GNSS-IR; POLARIS

TABLE OF CONTENTS

CHAPTER 1: Introduction

Accurate observation of ocean surface waves is essential for a wide range of scientific and practical applications, including marine safety, coastal engineering, climate studies, and operational oceanography. Wave conditions strongly influence ship navigation, offshore operations, and coastal processes, making reliable wave information a fundamental requirement in coastal and marginal seas.

A variety of techniques have been developed to observe ocean waves. In situ measurements, such as wave buoys and coastal wave gauges, provide high-quality measurements but remain spatially sparse and costly to deploy and maintain. Remote sensing techniques, including satellite altimetry and synthetic aperture radar (SAR), offer broad spatial coverage but are limited by revisit time and often lack the temporal resolution required to capture short-term wave variability.

Shipborne observations, particularly those obtained from vessels operating on regular routes, offer an attractive complementary approach by providing repeated measurements along fixed tracks, thereby filling observational gaps between fixed stations and satellite observations.

Despite their potential for providing in situ information, ship-borne wave observations face several fundamental challenges. Unlike satellite measurements, ship-based observations are not systematically designed for oceanographic monitoring, and their spatial coverage depends strongly

on shipping routes and operational conditions. As a result, although observations can be concentrated in high-demand regions such as major navigation corridors and coastal seas, the overall distribution remains irregular and difficult to standardize.

Another major limitation lies in the observational methodology itself. Most ship-borne wave information is still obtained through visual estimates by crew members, which inherently lack objectivity and reproducibility. While instrumental measurements can provide quantitative wave parameters, they generally require the installation of dedicated wave gauges or radar systems. Such instruments are costly, require regular maintenance, and are therefore only deployed on a limited number of vessels.

Furthermore, the ship environment poses additional technical constraints. During navigation, ship-generated wakes and flow disturbances can significantly contaminate wave measurements, restricting the locations on a vessel where sensors can be reliably installed. Consequently, the expansion of ship-based quantitative wave observations critically depends on the availability of low-cost, robust, and easily deployable sensing techniques.

In this context, Global Navigation Satellite System interferometric reflectometry (GNSS-IR) has been widely investigated as an environmental sensing technique, exploiting interference between direct and reflected GNSS signals. Beyond wave observations, GNSS-IR has been successfully applied to the monitoring of tidal variations, sea surface height, soil moisture, snow depth, and inland

water bodies.

More recently, GNSS-IR has been extended to shipborne platforms as a low-cost wave-gauge approach, demonstrating that navigation-grade GNSS receivers installed on operating vessels can retrieve wave-related information without dedicated wave sensors.

The reference study by Ichikawa et al. (2024) demonstrated the feasibility of estimating significant wave height and wave period from moving vessels using shipborne GNSS-IR observations. However, this study was designed as a proof-of-concept, and the validation was based on a limited number of representative sea-state cases.

The proposed method relies on several simplifying assumptions, including the availability of a sufficient number of low-elevation GNSS satellites to enhance interferometric effects and the use of an assumed wave spectrum to construct a simulated look-up table (LUT). Because only a small number of comparisons were available, these assumptions could not be statistically validated, and the robustness of the retrieval under diverse environmental conditions remained unclear.

The present thesis addresses these limitations by extending shipborne GNSS-IR wave observations from a proof-of-concept demonstration to a statistically robust multi-case analysis. Field data were collected on board the ferry New Camellia during repeated crossings of the Tsushima Strait from August 2023 to January 2024. A navigation-grade GNSS receiver recorded 20-Hz SNR time series in burst mode (120 s every hour), enabling the extraction of wave-induced high-frequency SNR variations while maintaining a manageable data volume.

The GNSS-IR-derived wave parameters are evaluated using an external wave hindcast dataset provided by the Japan Weather Association (POLARIS), which serves as an independent reference for wave height and wave period.

By extending the calibration and evaluation dataset from three to 90 cases, this thesis enables a quantitative assessment of systematic bias, environmental sensitivity, and the robustness of LUT-based calibration approaches. In addition, the dependence of retrieval performance on satellite elevation angle is systematically examined to identify conditions suitable for operational shipborne GNSS-IR wave monitoring.

The specific objectives of this thesis are as follows:

1. To extend the calibration and evaluation of GNSS-IR wave retrievals from 3 to 90 cases, covering a wide range of sea states and wind conditions, to examine more generalized applicability of the method.

2. To quantitatively investigate limitations associated with the LUT-based conversion. The remainder of this thesis is organized as follows. Chapter 2 describes the observational setup on board the New Camellia, the GNSS-IR data processing procedures, and the POLARIS Hindcast products used in this study. Chapter 3 presents the results of case studies and multi-case statistical analyses. Chapter 4 discusses systematic bias, calibration effects, and elevation-dependent performance characteristics. Chapter 5 summarizes the main conclusions and outlines prospects for future applications of shipborne GNSS-IR wave measurements.

Chapter 2 Materials and Methods

2.1 Review of the reference GNSS-IR wave-retrieval method

This thesis adopts the GNSS interferometric reflectometry (GNSS-IR) wave-retrieval framework of Ichikawa et al. (2024) as its methodological baseline, retaining the same physical interpretation and overall processing logic so that wave parameters are derived under an equivalent premise. The primary extension of the present work lies in the evaluation design: rather than demonstrating feasibility with only a small number of illustrative cases, the assessment is expanded to a substantially larger set of cases (e.g., 90 cases) to enable a more robust multi-case evaluation.

Accordingly, Section 2.1 reviews the reference framework in a concise but defensible manner, providing the conceptual rationale and the key practical steps required for implementation. The controlled differences in observational and evaluation design between the reference study and this thesis are addressed separately in Section 2.2.

2.1.1 Conceptual basis in the reference study

Ichikawa et al. (2024) interpret shipborne GNSS-IR as an interference-based sensing technique in which the receiver records a composite signal comprising a direct GNSS component and a sea-surface-reflected component. After removing slowly varying contributions (primarily driven by satellite geometry and antenna gain), the remaining detrended SNR exhibits rapid oscillations. The reference study treats these oscillations as a direct manifestation of the evolving interferometric phase associated with the direct–reflected signal combination.

A central concept emphasized in the reference framework is that, over a satellite pass, the satellite elevation changes smoothly and (locally) monotonically. This provides a convenient geometric viewpoint: the oscillatory behaviour of detrended SNR can be interpreted in relation to the satellite-elevation evolution along an arc, enabling consistent interpretation across different satellite tracks rather than treating the oscillations as arbitrary time-domain fluctuations.

Within this geometric viewpoint, sea-surface variability perturbs the effective reflection geometry and consequently modulates the interferometric behaviour. Ichikawa et al. (2024) propose that such modulation is detectable through the oscillation density of detrended SNR: more energetic sea states tend to produce more frequent oscillatory crossings, while calmer conditions yield less frequent crossings. This motivates the use of a compact oscillation-density metric (the crossing number) and, importantly, highlights the need to account for elevation-related geometric effects so that estimates are comparable across satellite arcs with different elevation ranges.

Finally, the reference study recognises that, under realistic multi-frequency sea states, a fully analytical mapping from an oscillation-density index to standard wave parameters is not straightforward. Therefore, it adopts a simulation-assisted strategy: numerical sea-surface realisations are used to calibrate a look-up table linking the oscillation-density behaviour (after geometric treatment) and wave-period information to significant wave height. This conceptual design leads naturally to the practical workflow summarized next.

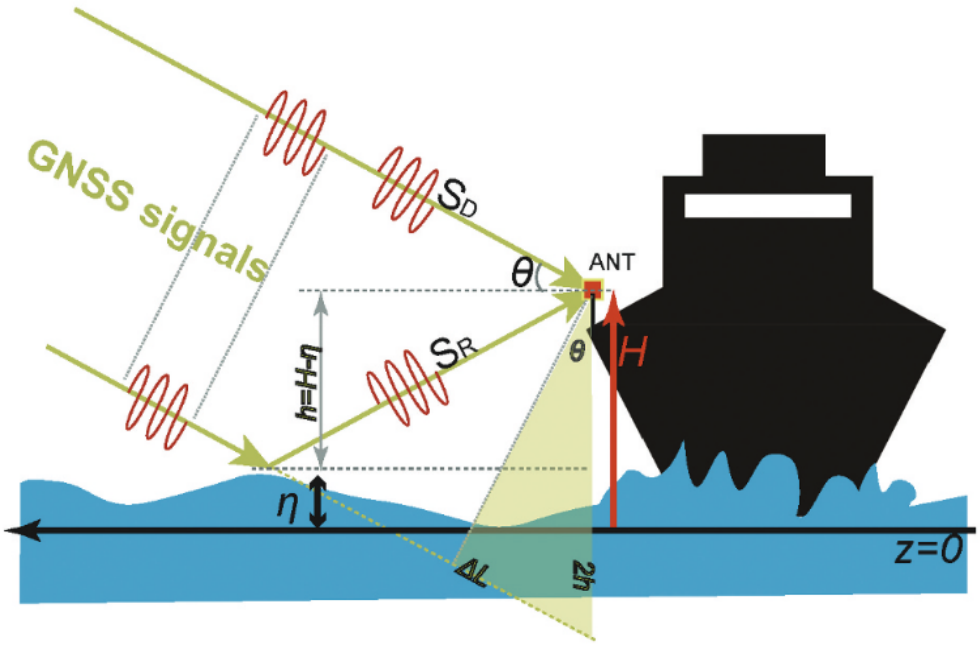

Fig. 2-1 Schematic diagram of shipborne GNSS reflectometry used in the GNSS-IR framework. (after Ichikawa et al., 2024)

2.1.2 Practical estimation procedure in the reference framework

Fig. 2-2 summarizes the end-to-end GNSS-IR processing and validation workflow adopted in this thesis following Ichikawa et al. (2024): high-rate shipborne GNSS SNR observations are detrended to isolate the rapidly varying interference component; crossing-number indices are computed over prescribed windows; wave period and significant wave height are then obtained within the reference retrieval logic and evaluated against external wave information.

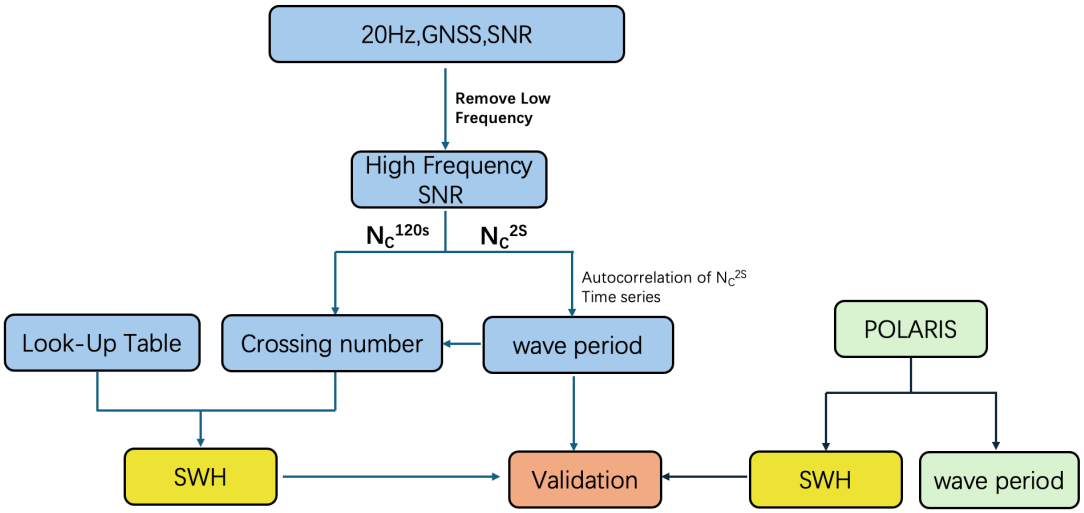

Fig. 2-2 Flowchart of the GNSS-IR wave-retrieval and validation workflow used in this thesis. (after Ichikawa et al., 2024)

(1) Detrending to isolate the oscillatory component

The raw SNR contains both slowly varying contributions (satellite geometry and antenna gain) and rapidly varying oscillations associated with the interference between direct and reflected signals. The reference method removes the low-frequency baseline and retains the oscillatory component for wave estimation:

$$\mathrm{SNR}'(t) = \mathrm{SNR}(t) - \widehat{\mathrm{SNR}}_{\mathrm{trend}}(t). \qquad (2\text{-}1)$$

(2) Oscillation-density index (crossing number) and elevation-geometry treatment

To quantify how "dense" the oscillations are, Ichikawa et al. (2024) use a crossing-number metric: within a predefined window, the number of intersections between $\mathrm{SNR}'(t)$ and multiple reference levels is counted and averaged to obtain a robust oscillation-density index.

Because oscillation behaviour depends systematically on satellite elevation through GNSS-IR geometry, the metric is further normalized by $\sin\theta$ to reduce arc-to-arc variability:

$$\widetilde{N}_c = \frac{N_c}{\sin\theta}, \qquad (2\text{-}2)$$

where θ is the satellite elevation angle and $\widetilde{N}_c$ denotes the geometry-reduced oscillation-density index. Adequate sampling must also be ensured (given the adopted sampling rate) so that the oscillations are resolvable and not aliased.

(3) Two-stage retrieval: period first, then height via LUT

The reference framework retrieves wave parameters in two steps. First, a short-window crossing-number sequence is formed and its temporal structure is analysed using an autocorrelation approach; the lag of the first prominent autocorrelation peak is taken as the significant wave period estimate T_g. Second, a long-window oscillation-density index is evaluated (with elevation-geometry treatment) and combined with the estimated period. The significant wave height is then obtained by querying a simulation-based LUT constructed from multi-frequency random sea-surface realisations:

$$\mathrm{SWH} = \mathrm{LUT}\left(T_g, \widetilde{N}_c\right). \qquad (2\text{-}3)$$

This implementation is well suited for defense presentation: T_g is derived from the periodicity in the oscillation-density metric, while SWH is obtained through a calibrated mapping that accounts for realistic sea-state variability.

2.2 Difference from the reference study: datasets, study design, and scope of extensions

Different from Ichikawa et al. (2024), who demonstrated the feasibility of shipborne GNSS-IR wave retrieval using a limited number of representative cases (three cases), this thesis extends the evaluation to a substantially larger dataset (90 cases) to examine robustness under more diverse conditions. Importantly, this extension is achieved without changing the core retrieval methodology: the same baseline algorithmic components (crossing-number metric for high-frequency SNR oscillations, elevation-angle normalisation, autocorrelation-based wave-period estimation, and LUT-based SWH retrieval) are retained to ensure direct comparability with the reference framework.

Although this section focuses on “differences”, it is also necessary to clarify the common data sources used in both the reference study and this thesis. Both studies are built on (i) shipborne high-rate GNSS SNR observations as the primary input for GNSS-IR wave retrieval and (ii) an external wave dataset as a benchmark for validation. In this thesis, the GNSS-IR estimates are evaluated against co-located outputs from the Japan Weather Association (JWA) POLARIS hindcast wave products, specifically significant wave height (SWH) and wave period, downloaded from the official JWA POLARIS Hindcast portal: (https://polaris.jwa.or.jp/hindcast/login).

Different from the reference study in terms of the observation platform and route, this thesis uses shipborne GNSS observations collected on the international ferry New Camellia (Fig.2-3) along the operational Hakata (Japan)–Busan (Korea) route across the Tsushima Strait (Fig.2-4), enabling repeated crossings along a geographically consistent transect. This repeated-transect design is a key reason why the present work can expand from a small feasibility demonstration to a multi-case evaluation while maintaining comparable spatial context across cases.

Fig. 2-3 The international ferry New Camellia, which served as the observation platform.
(Retrieved from: https://idyllicocean.com/vdb/ship18_pic_info.php?p_id=2344)

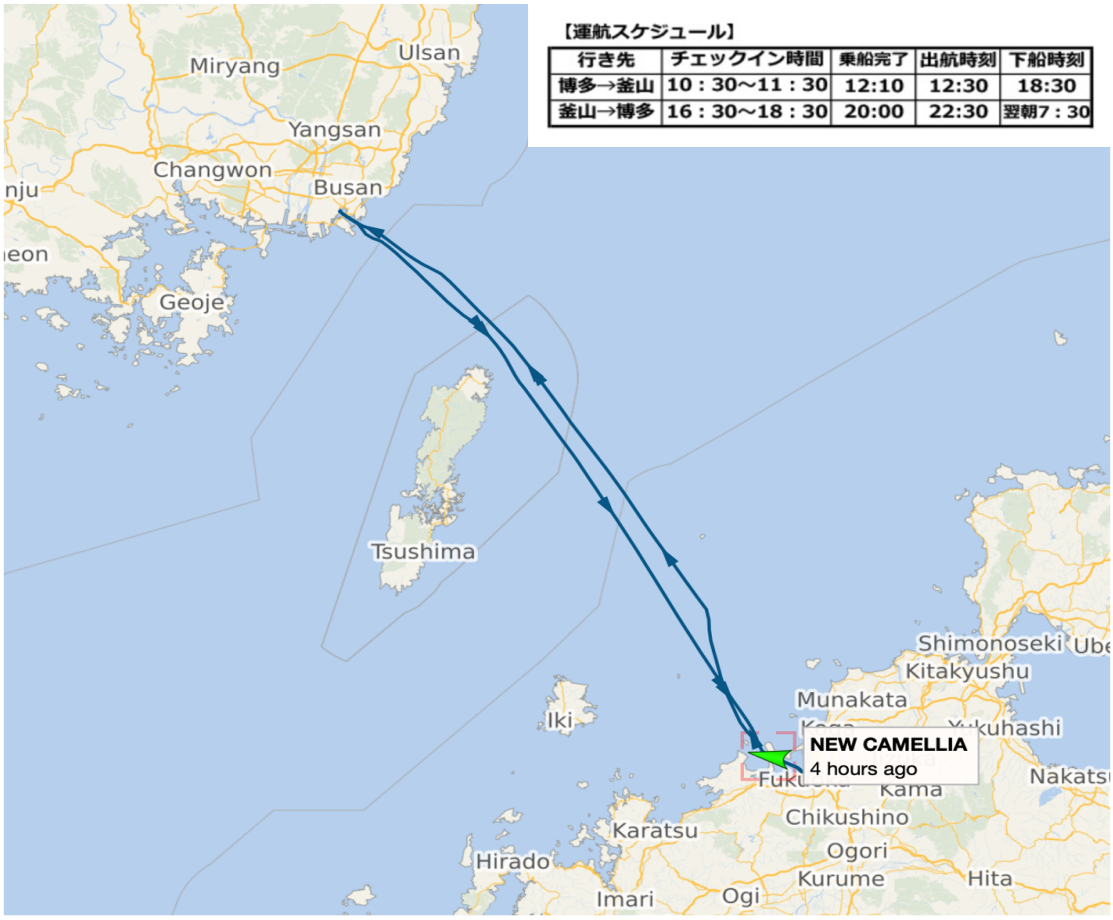

Fig. 2-4 Study area and operational route across the Tsushima Strait between Hakata (Japan) and Busan (Korea).

(Retrieved from: https://www.vesselfinder.com/?imo=9304497)

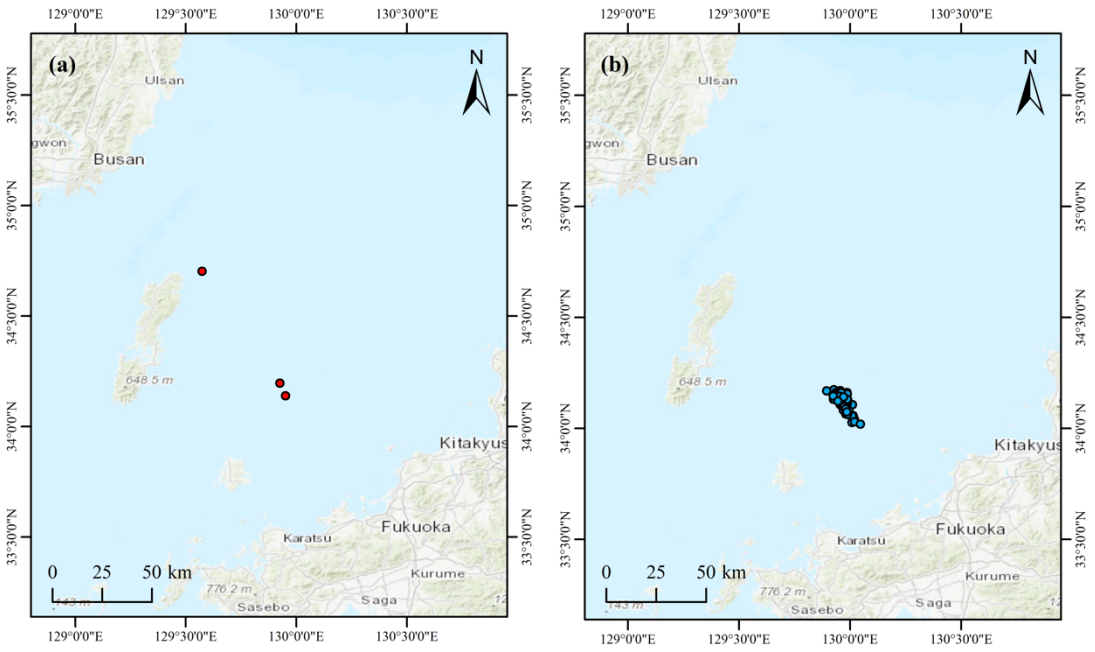

Fig.2-5 Comparison of data points in Ichikawa et al. (left) and the present study (right)

Different from the reference study in terms of the GNSS sampling strategy and observation design, this thesis adopts a structured observation scheme to support systematic accumulation of comparable cases: 20 Hz SNR sampling using 120 s bursts every hour, incorporating multi-constellation observations, spanning 1 Aug 2023–29 Jan 2024, with mid-leg sampling times (UTC 05:10/18:10) and analysis windows designed for variability assessment (approximately ~3-day windows) (Table 2-1).

GNSS-IR Observation Date and Time (UTC)

2023-08-01 18:10	2023-08-02 05:10	2023-08-04 18:10	2023-08-05 05:10	2023-08-07 18:10	2023-08-08 05:10
2023-08-13 18:10	2023-08-14 05:10	2023-08-16 18:10	2023-08-17 05:10	2023-08-19 18:10	2023-08-20 05:10
2023-08-22 18:10	2023-08-23 05:10	2023-08-25 18:10	2023-08-26 05:10	2023-08-28 18:10	2023-08-29 05:10
2023-09-01 18:10	2023-09-02 05:10	2023-09-04 18:11	2023-09-05 05:11	2023-09-07 18:11	2023-09-08 05:11
2023-09-13 18:11	2023-09-14 05:11	2023-09-16 18:11	2023-09-17 05:11	2023-09-19 18:11	2023-09-20 05:11
2023-09-22 18:11	2023-09-23 05:11	2023-09-25 18:11	2023-09-26 05:11	2023-09-28 18:11	2023-09-29 05:11
2023-10-01 18:12	2023-10-02 05:13	2023-10-04 18:12	2023-10-05 05:12	2023-10-07 18:12	2023-10-08 05:12
2023-10-13 18:12	2023-10-14 05:12	2023-10-16 18:12	2023-10-17 05:12	2023-10-19 18:12	2023-10-20 05:12
2023-10-22 18:12	2023-10-23 05:12	2023-10-25 18:12	2023-10-26 05:12	2023-10-28 18:12	2023-10-29 05:12
2023-11-01 18:13	2023-11-02 05:13	2023-11-04 18:13	2023-11-05 05:13	2023-11-07 18:13	2023-11-08 05:13
2023-11-13 18:13	2023-11-14 05:13	2023-11-16 18:13	2023-11-17 05:13	2023-11-19 18:13	2023-11-20 05:13
2023-11-22 18:13	2023-11-23 05:13	2023-11-25 18:13	2023-11-26 05:13	2023-11-28 18:13	2023-11-29 05:13
2023-12-01 18:13	2023-12-02 05:13	2023-12-04 18:13	2023-12-05 05:14	2023-12-07 18:14	2023-12-08 05:14
2023-12-13 18:14	2023-12-14 05:14	2023-12-16 18:14	2023-12-17 05:14	2023-12-19 18:14	2023-12-20 05:14
2023-12-22 18:14	2023-12-23 05:14	2023-12-25 18:14	2023-12-26 05:14	2023-12-28 18:14	2023-12-29 05:14
2024-01-01 18:14	2024-01-02 05:14	2024-01-04 18:14	2024-01-05 05:14	2024-01-07 18:14	2024-01-08 05:14
2024-01-13 18:11	2024-01-14 05:11	2024-01-16 18:11	2024-01-17 05:11	2024-01-19 18:10	2024-01-20 05:11
2024-01-22 18:10	2024-01-23 05:10	2024-01-25 18:10	2024-01-26 05:10	2024-01-28 18:10	2024-01-29 05:10

Table 2-1 GNSS-IR Observation Date and Time (UTC)

The clustering of data points in Fig. 2-5 (right) reflects the structured observation design adopted in this study rather than a limitation of spatial coverage. All GNSS-IR observations were collected along a fixed, repeatedly operated ferry route, and analysis epochs were selected at consistent mid-leg positions to minimize coastal and harbor influences and to ensure better consistency and accuracy in comparison with the POLARIS Hindcast data.

While the reference study also used 20 Hz SNR in a shipborne GNSS-IR configuration, these practical settings define how the 90 GNSS datasets are formed and ensure that all cases are processed under consistent conditions.

Finally, different from a small-number feasibility demonstration, this thesis emphasises systematic validation and stratified multi-case analyses enabled by the expanded case set (90 GNSS datasets), including (where relevant) stratification by observational factors such as satellite elevation ranges and quality-control assessments. These analyses aim to identify the conditions under which the reference GNSS-IR approach performs robustly and those under which performance degrades.

Table 2-2 summarizes which elements are kept consistent with Ichikawa et al. (2024) and which elements are extended or modified in this thesis, clarifying that the contribution of this work is an expanded evaluation on a repeated operational transect rather than a modification of the underlying GNSS-IR retrieval methodology.

Aspect	Ichikawa et al. (2024)	This thesis	Different from Ichikawa?
Observation platform and route	Shipborne GNSS observations acquired on an operational vessel (as described in Ichikawa et al., 2024).	Shipborne GNSS observations acquired on the international ferry New Camellia along the operational Hakata (Japan)–Busan (Korea) route across the Tsushima Strait (Fig. 2.4), providing repeated crossings along a geographically consistent transect.	Yes
GNSS sampling strategy	20 Hz SNR observations of low-elevation satellites in a shipborne GNSS-IR configuration.	20 Hz SNR sampling (120 s bursts every hour); multi-constellation; 1 Aug 2023–29 Jan 2024; UTC 05:10/18:10 (mid-leg sampling); ~3-day windows for variability analysis.	Partly (sampling rate consistent; observation scheme differs)
Core retrieval algorithm	Crossing-number metric; elevation-angle normalisation; autocorrelation-based wave-period estimation;	Same algorithmic components are adopted to ensure methodological consistency and comparability with the reference study.	No

Aspect	Ichikawa et al. (2024)	This thesis	Different from Ichikawa?
	LUT-based SWH retrieval.		
Numerical simulation and LUT	Multi-frequency random sea-surface simulation (ISSC / modified Pierson–Moskowitz spectrum) to construct a LUT linking crossing number and wave period to SWH.	Same LUT construction procedure is used; the resulting LUT is applied to the expanded observation set.	No
External reference for validation	POLARIS hindcast wave products (SWH and wave period) used to validate GNSS-IR estimates.	POLARIS hindcast wave products (SWH and wave period) are used as the primary external reference; data are obtained from the official JWA POLARIS portal.	No (same reference dataset; acquisition is documented)
Evaluation design and outputs	Feasibility demonstrated mainly through a small number of case studies (3 representative cases).	Multi-season, multi-case evaluation using 90 GNSS datasets, including stratified analyses (e.g., by satellite elevation) and quality-control assessments.	Yes

Table 2-2. Summary of methodological elements retained from Ichikawa et al. (2024) and elements extended or modified in this study.、

Chapter 3 Results

This chapter evaluates the performance of GNSS-IR–derived significant wave height (SWH) through a systematic comparison with the POLARIS hindcast data. Representative epochs are first presented to illustrate how the GNSS-IR wave parameters (dominant wave period, and SWH) behave under different satellite-availability scenarios. The overall bias characteristics are then quantified using all available epochs after applying the elevation-angle filter (elevation < 15°). Finally, an empirical SWH-dependent calibration is introduced, and its effectiveness is assessed using both visual diagnostics and statistical metrics (correlation coefficient, RMSE, and R-square).

3.1 Satellites availability

We first examine the availability of low-elevation satellites. Because the distribution of GNSS satellites changes in time, and the GNSS antennas have been set only on the right side of the ship, we may miss the other half of GNSS satellites. Because GNSS-IR requires low-elevation satellites, it is important to examine whether low-elevation satellites are always available or not.

This section presents two representative epochs to demonstrate the behavior of GNSS-IR wave-parameter estimation at the epoch scale. The two cases are selected to contrast a multi-satellite scenario and a single-satellite scenario under the same elevation-angle constraint (elevation < 15°). For each epoch, the blue markers represent GNSS-IR estimates derived from individual satellite tracks, whereas the orange star indicates the POLARIS reference at the same epoch.

Figure 3-1 shows a multi-satellite example (2023/11/02 03:10:00 UTC) in which multiple satellites contribute independent reflection geometries within the epoch. Although the GNSS-IR

estimates span a range of Tg–SWH combinations, the SWH values remain consistently lower than the POLARIS reference, indicating systematic underestimation even when multiple satellite tracks are available for cross-checking within the same epoch. The spread among satellites reflects geometry- and track-dependent variability in the observable, but the common tendency to fall below the reference suggests that the dominant bias is systematic rather than purely random inter-satellite noise.

Figure 3-2 provides a contrasting single-satellite example (2024/01/20 14:10:00 UTC). In this case, GNSS-IR wave parameters are determined from one satellite track only, without the benefit of inter-satellite averaging. Despite the reduced sampling, the derived SWH is still markedly smaller than the POLARIS reference, consistent with the multi-satellite example.

The consistency of SWH underestimation in both multi-satellite and single-satellite cases indicates that the observed bias is not primarily caused by satellite sampling density or inter-satellite inconsistencies. Instead, it suggests that the underestimation reflects a systematic characteristic of the GNSS-IR wave height retrieval under the current processing framework. These example cases motivate a comprehensive evaluation of GNSS-IR SWH performance using the full dataset.

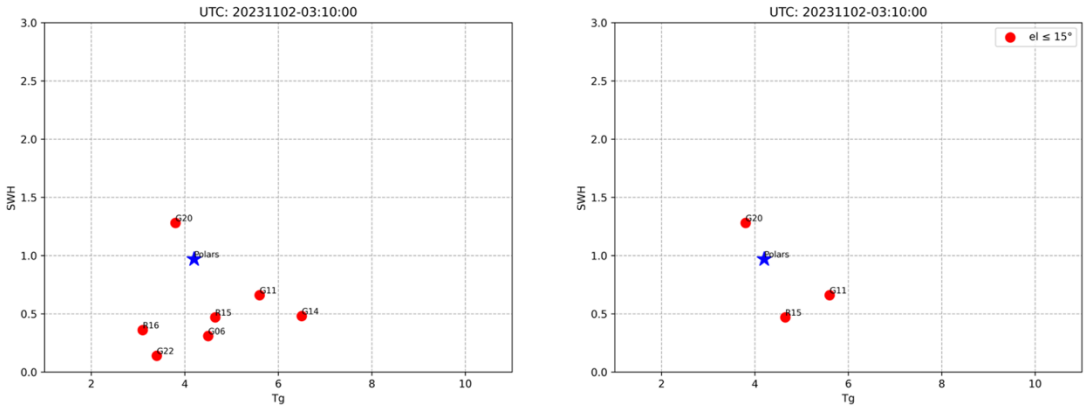

Figure 3-1. Example of GNSS-IR–derived Tg and SWH from multiple satellites at a single epoch (2023/11/02 03:10:00 UTC). (Red markers) per-satellite GNSS-IR estimates; (Blue star) POLARIS reference

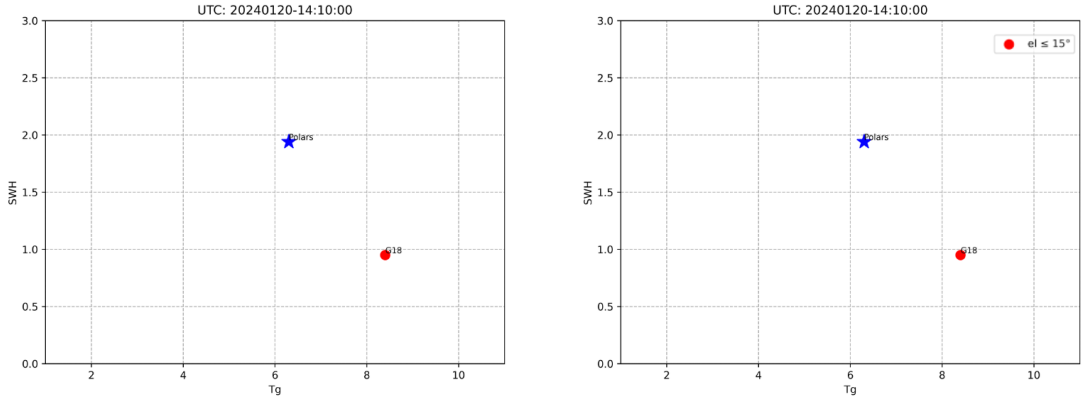

Figure 3-2. Example of GNSS-IR–derived Tg and SWH from multiple satellites at a single epoch (2024/01/20 14:10:00 UTC). (Red markers) per-satellite GNSS-IR estimates; (Blue star) POLARIS reference.

Table 3-1 summarizes satellite availability per epoch after applying the elevation-angle filter. It is noticeable that no low-elevation satellites are available in 30% of cases, suggesting that GNSS-IR is not applicable. Cases that have more than two low-elevation satellites, as used in Ichikawa et al. (2024), are found only 52% of cases.

Number of Satellites	Number of cases	Percentages
0	28	30.43%
1	16	17.39%
2	25	27.17%
3	14	15.22%
4	3	3.26%
5	5	5.43%
6	1	1.09%

Table 3-1. Distribution of the number of GNSS satellites per epoch after elevation-angle filtering (elevation < 15°)

3.2 Significant Wave Height (SWH) Comparisons

To quantify the overall performance of GNSS-IR wave-height estimation, all available epochs passing the elevation-angle filter (elevation < 15°) and contain at least two satellites are compiled and compared with the POLARIS reference. For each epoch, multiple per-satellite GNSS-IR estimates (if available) are aggregated into a single epoch-level value by averaging across satellites, yielding a per-epoch mean GNSS-IR SWH that can be compared consistently to the POLARIS SWH.

Figure 3-3 presents the scatter comparison between GNSS-IR per-epoch mean SWH and POLARIS SWH. The relationship is weak ($r = 0.137$; R-square = 0.019), and most points lie below the one-to-one line, demonstrating a systematic underestimation of SWH by GNSS-IR across the observed sea-state range. The RMSE is 0.740 m, indicating that the discrepancy is substantial relative

to typical wave heights in this dataset. The regression slope is notably smaller than unity, further confirming that the bias is systematic rather than a purely random error component.

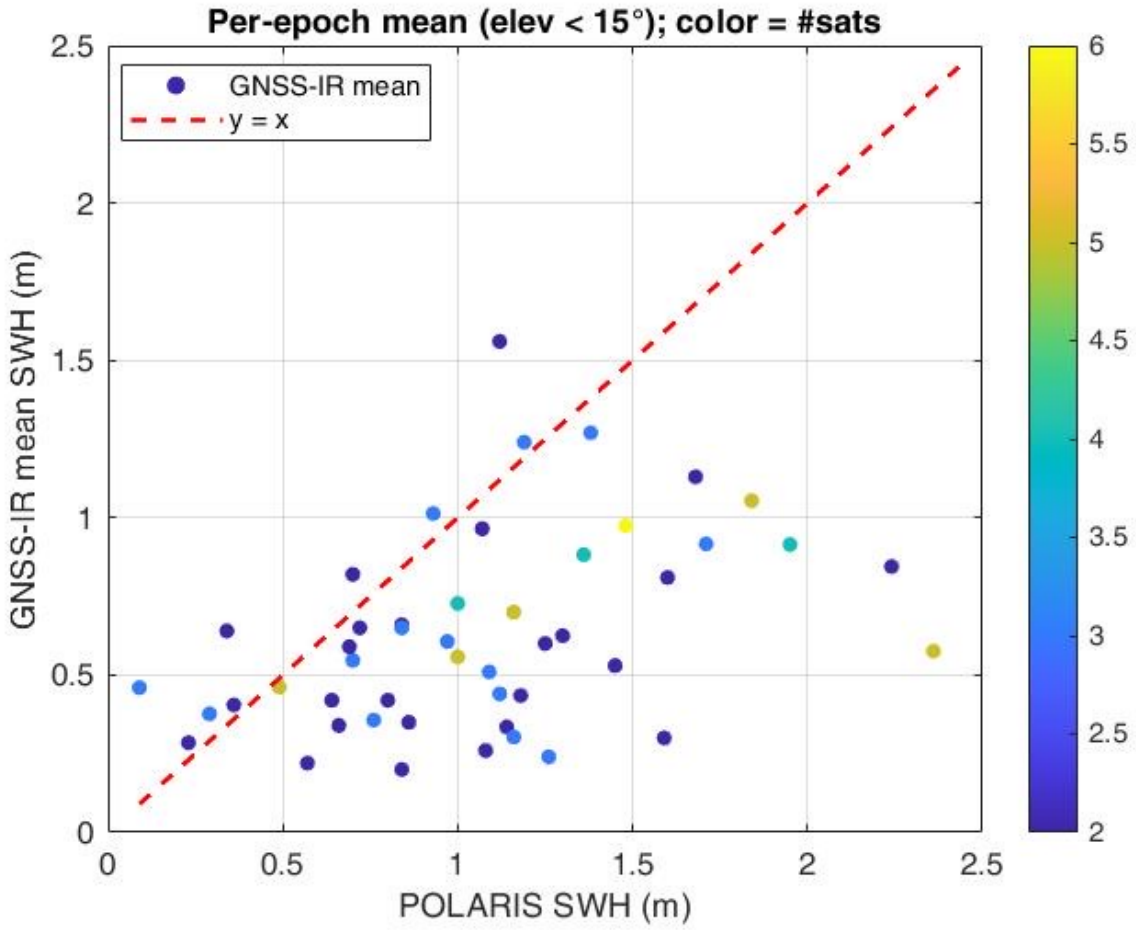

Figure 3-3. Comparison between GNSS-IR and POLARIS significant wave height Scatter comparison between GNSS-IR per-epoch mean SWH and POLARIS SWH (elevation < 15°and satellite ≥2). The red dashed line indicates the one-to-one relationship

3.3 Correction Factors

To mitigate the systematic underestimation identified in Section 3.2, an empirical SWH-dependent calibration is introduced. The central idea is to derive a correction factor as a function of sea state (represented by POLARIS SWH) and then apply it to the GNSS-IR SWH estimates. Importantly, this calibration adjusts the SWH scale while keeping the normalized crossing number (Nc) definition unchanged, thereby preserving the original GNSS-IR observable formulation.

First, POLARIS SWH is discretized into 0.5 m intervals. Within each interval, paired epoch-level values (POLARIS SWH and GNSS-IR per-epoch mean SWH) are collected to estimate representative values for that sea state. To reduce the influence of sporadic retrieval failures and heavy-tailed errors, outliers are removed using a robust criterion, i.e. MAD-based screening on the residual GNSS–POLARIS difference, and representative bin values are computed using an outlier-resistant statistic (e.g., trimmed mean). Figure 3-4 illustrates the representative GNSS-IR and POLARIS SWH values across the 0.5 m intervals, showing that the GNSS-IR underestimation generally increases with sea state.

A multiplicative correction factor is then defined for each SWH interval as the ratio between the representative POLARIS SWH and the representative GNSS-IR SWH (factor = POLARIS / GNSS). Figure 3-5 shows the resulting bin-wise factors, together with the sample size in each bin. Because bin-wise factors form a step function, the factor sequence is further interpolated into a continuous function of SWH (e.g., using a shape-preserving cubic interpolation) to avoid artificial discontinuities when applying the correction and when updating the look-up table.

The factor function is applied to GNSS-IR SWH to obtain corrected estimates. Figure 3-6 compares the per-epoch SWH before and after calibration against POLARIS. After applying the SWH-dependent factors, agreement improves substantially: r increases from 0.137 to 0.678, RMSE decreases from 0.740 m to 0.535 m, and R-square increases from 0.019 to 0.460. These improvements indicate that the proposed calibration effectively reduces the dominant systematic bias, although residual scatter remains, particularly at higher wave heights, suggesting that factors beyond a simple

sea-state-dependent scaling (e.g., geometry, wind, and real-observation effects on Nc) may still contribute to the remaining variability.

Finally, the same correction strategy can be propagated to the original Nc–SWH look-up table (LUT) by adjusting the LUT SWH values using the continuous factor function while keeping the Nc axis unchanged. Figure 3-7 compares the original LUT, the bin-wise corrected LUT, and the smoothed corrected LUT, demonstrating that factor smoothing restores a smooth LUT shape comparable to the original while incorporating the empirically derived sea-state dependence.

To further evaluate the LUT-based correction, the corrected LUT shown in Fig. 3-7 was applied to the GNSS-IR observations to obtain LUT-corrected SWH estimates. Fig. 3-8 compares the LUT-corrected GNSS-IR SWH with the POLARIS SWH.

The LUT-based correction also improves the agreement relative to the original estimates, although the improvement is more moderate than that obtained using the direct POLARIS-referenced scaling. The correlation coefficient increases to $r = 0.389$ ($R^2 = 0.151$), and the RMSE decreases to 0.598 m. These results indicate that the empirically corrected LUT partially compensates for the systematic underestimation while avoiding the direct use of POLARIS values for each individual epoch.

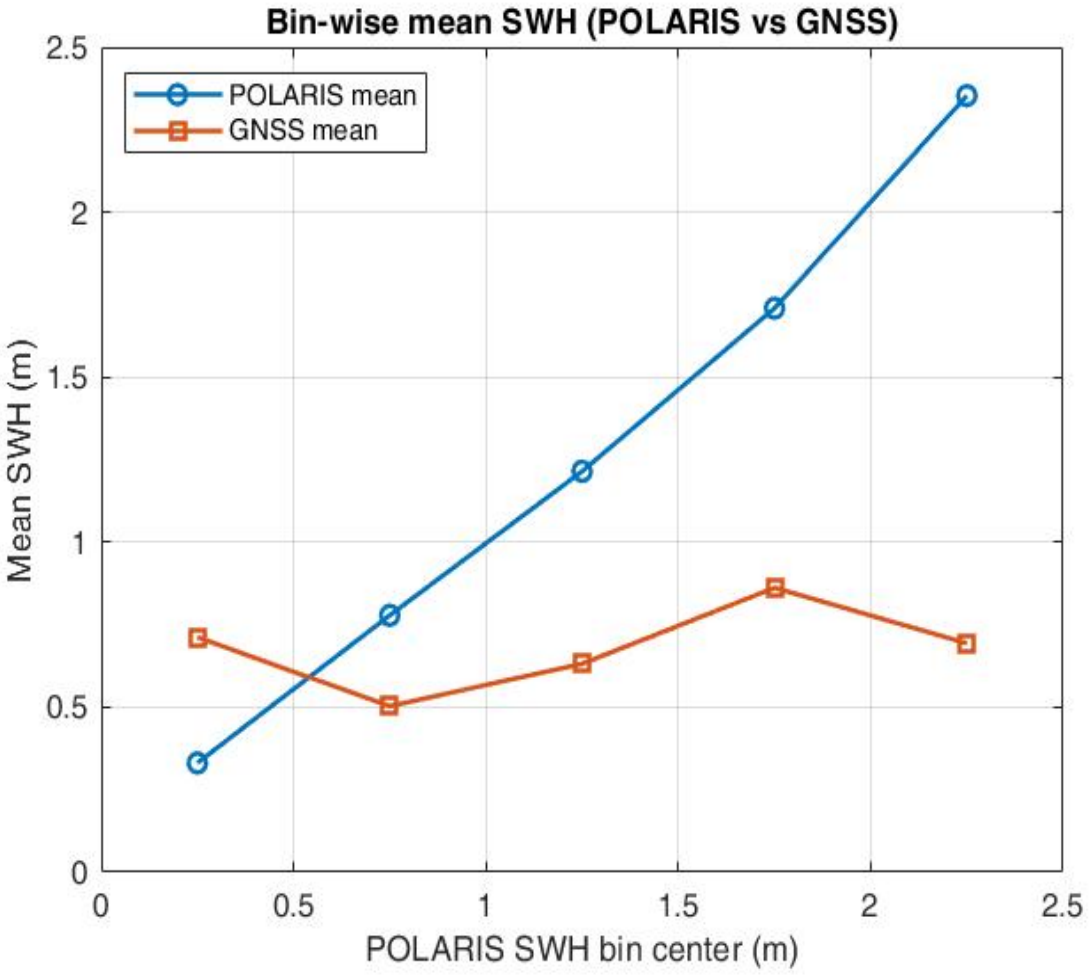

Figure 3-4. Bin-wise mean values of SWHs from GNSS-IR and POLARIS datasets

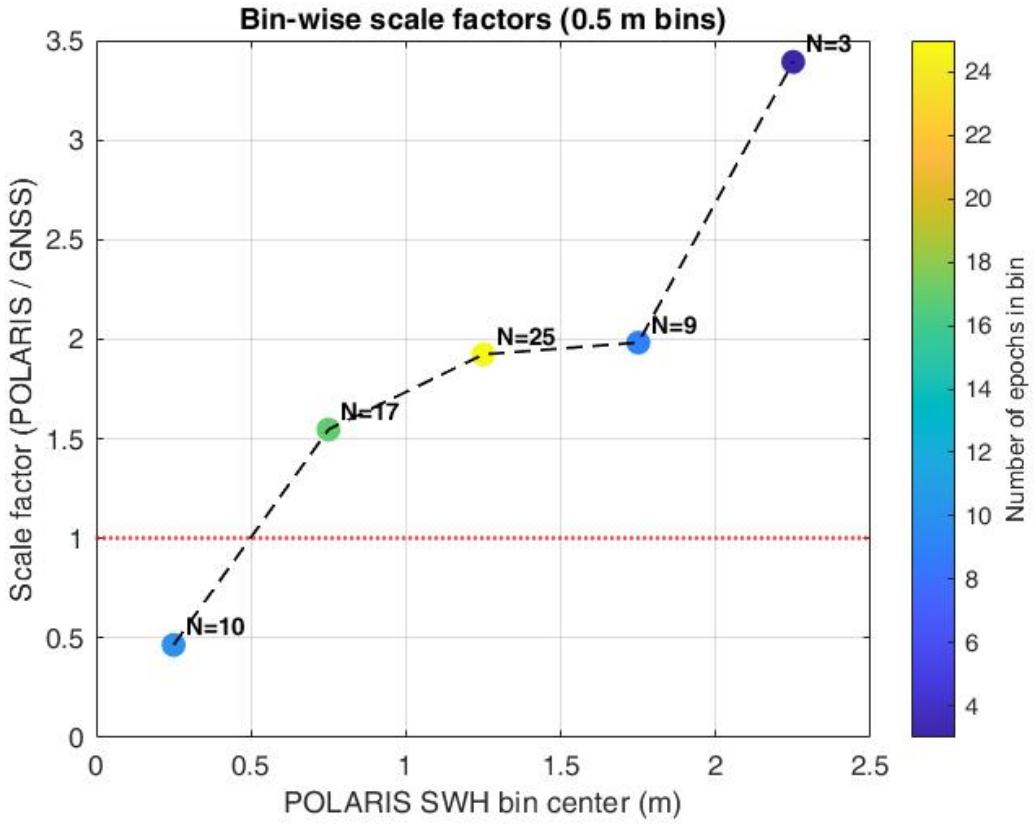

Figure 3-5. SWH-dependent multiplicative correction factors (POLARIS/GNSS) derived from 0.5 m SWH intervals. Numbers indicate the number of epochs in each interval.

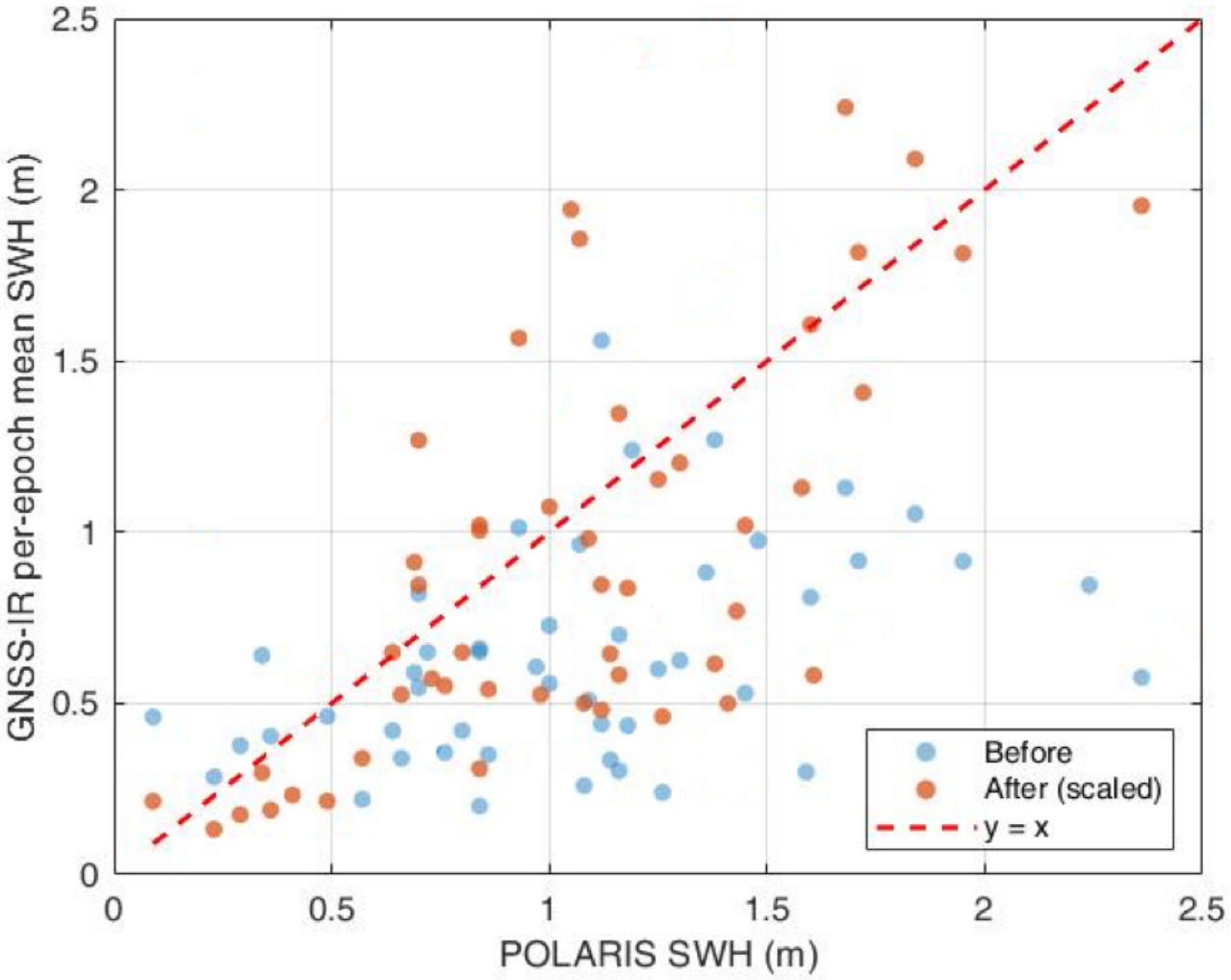

Figure 3-6. Comparisons before and after empirical factor corrections. (Blue dots) SWHs before correction; (Orange dots) SWHs after corrections

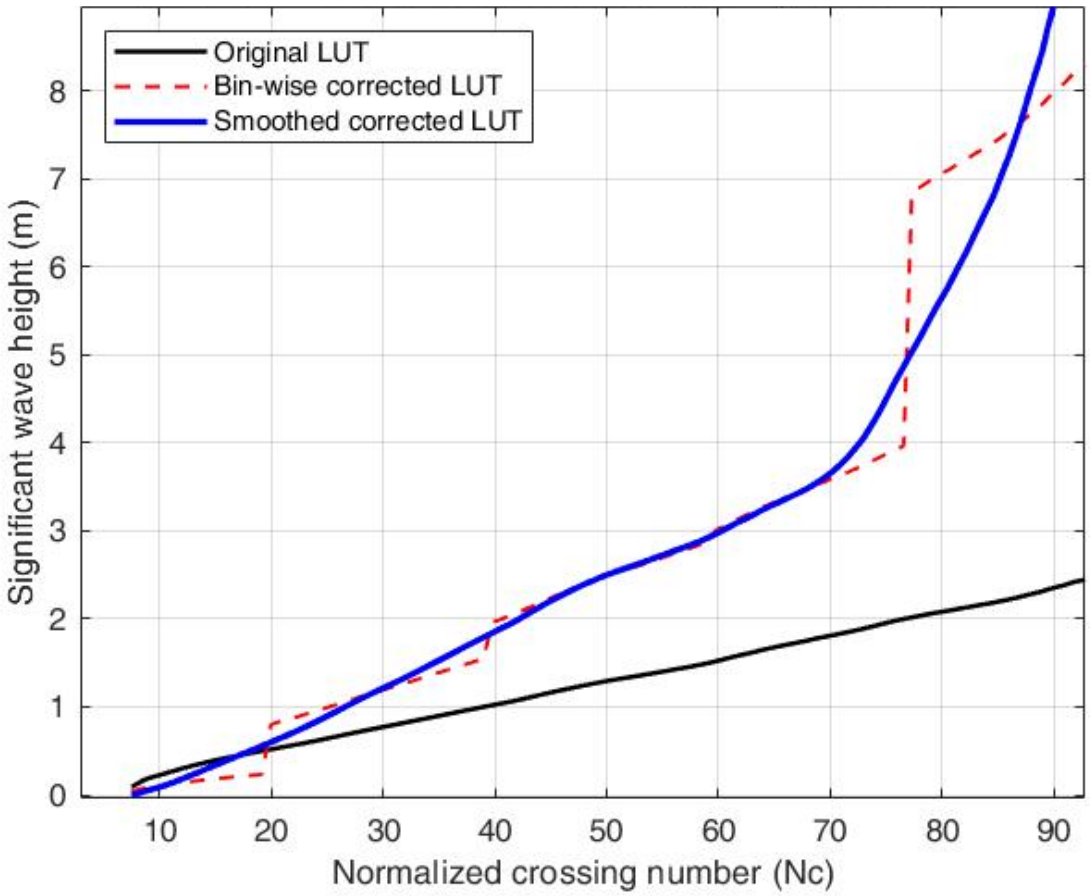

Figure 3-7. Look-up table (Nc–SWH) comparison: original LUT (black), bin-wise corrected LUT (red), and smoothed corrected LUT (blue).

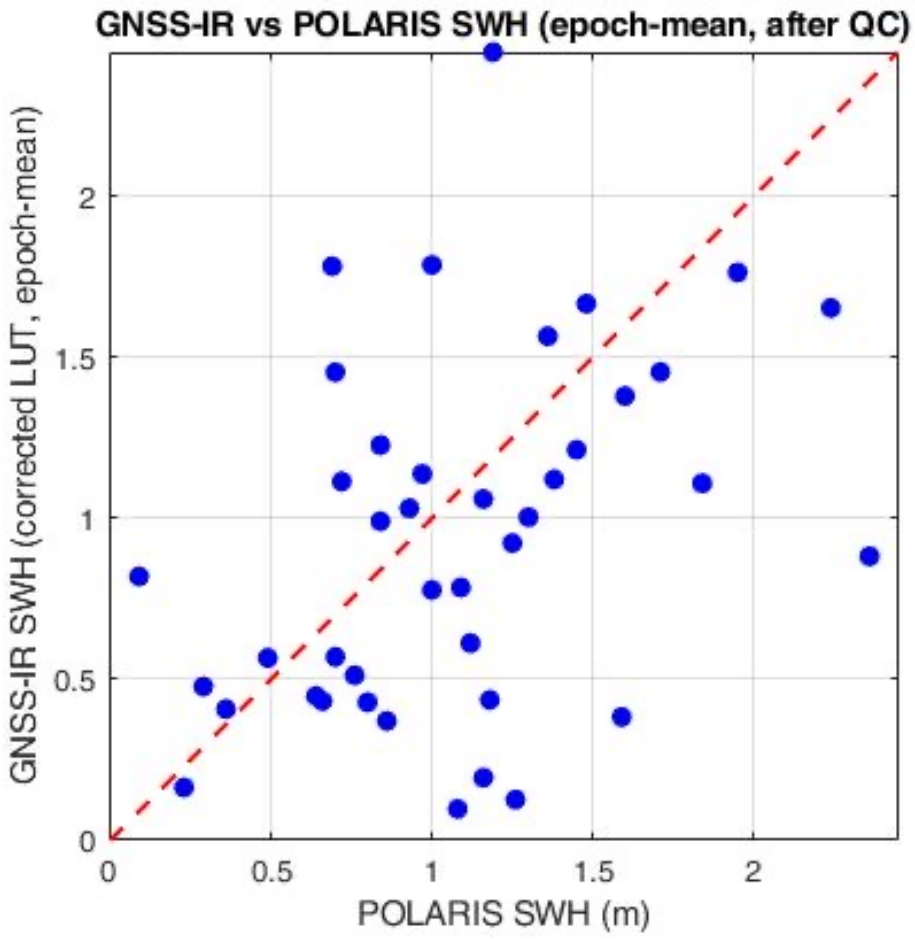

Figure 3-8. Comparison between LUT-corrected GNSS-IR SWH and POLARIS SWH. The GNSS-IR estimates were converted using the corrected LUT derived from the bin-wise analysis (Fig. 3-7).

3.4 Chapter Summary

This chapter evaluated GNSS-IR–derived SWH by comparing epoch-level estimates against the POLARIS Hindcast data. Representative multi-satellite and single-satellite examples demonstrated consistent SWH underestimation, indicating that the bias is not primarily controlled by satellite availability within an epoch. A dataset-wide comparison confirmed the systematic nature of the underestimation, with weak correlation and large RMSE relative to POLARIS.

To address this limitation, an empirical calibration based on SWH-dependent correction factors was developed. By binning POLARIS SWH into 0.5 m intervals, estimating robust representative values within each interval, and applying multiplicative correction factors, the agreement with POLARIS improved markedly in terms of r, RMSE, and R-square. A smoothed factor function was further used to update the Nc–SWH LUT while maintaining a smooth LUT shape comparable to the original one. Despite these improvements, residual scatter remains, especially at higher sea states, highlighting the need for future work to enhance the physical sensitivity and robustness of the underlying GNSS-IR observables under real ocean conditions.

Chapter 4 Discussions

4.1 Satellite Availability

Only satellites with low elevation angles provide reflection geometries that are sufficiently sensitive to sea surface height variations. The present study reveals that nearly half of the cases have less than two low-elevation satellites. Attempts to increase data availability by including higher-elevation satellites were found to be ineffective. High-elevation signals exhibit weaker interference patterns and reduced sensitivity to vertical sea surface displacements, thereby violating the physical assumptions underlying GNSS-IR. As a result, simply expanding the elevation-angle range does not resolve the limitation of insufficient observations.

A more practical solution would be to set another antenna on the other side of the ship so that both sides of GNSS satellites can be used.

These results emphasize that observation geometry plays a dominant role in determining the feasibility of shipborne GNSS-IR and must be carefully considered when designing operational wave-monitoring systems.

4.2 Physical Origins of Systematic Underestimation in GNSS-IR–Derived SWH

A consistent underestimation of significant wave height (SWH) was observed in GNSS-IR results when compared with POLARIS reference measurements. This bias persists across different observation periods and satellite configurations, indicating that it cannot be attributed solely to random noise or insufficient sampling.

One major source of underestimation arises from the assumptions embedded in the look-up table (LUT) used to convert normalized crossing numbers to SWH. The LUT is constructed based on idealized wave spectral models, which implicitly assume stationary and homogeneous sea states. In real ocean environments, wave spectra vary substantially with wind conditions, fetch, and swell dominance. Deviations from the assumed spectral shape alter the relationship between surface roughness statistics and wave height, leading to systematic bias when a single LUT is applied universally.

More importantly, under energetic sea states, the dominant wavelength may become comparable to or exceed the characteristic length scale of the vessel. In such cases, the vessel no longer acts as a stationary observation platform. Instead, it responds dynamically to wave forcing and moves approximately in phase with the surrounding sea surface. This behavior directly violates a key assumption of GNSS-IR, namely that sea surface elevation changes dominate the reflected signal while antenna motion remains negligible.

When vessel motion becomes significant, part of the sea surface signal is effectively absorbed by the platform itself, reducing the relative height variation sensed by the reflected signal. As a

consequence, GNSS-IR measurements increasingly underestimate true wave height as sea state intensifies. This underestimation therefore reflects a physical limitation of the sensing principle rather than a deficiency in data processing.

The above discussions suggest that combination of GNSS-IR–based sea surface sensing and direct GNSS-based vessel motion sensing can cover the whole range of SWH. Under calm to moderate sea conditions, vessel motion is limited, and GNSS-IR effectively captures sea surface height variations through reflected signal interference. In this regime, GNSS-IR provides meaningful and physically interpretable wave height estimates.

As sea conditions become rougher, however, vessel motion increasingly dominates the vertical displacement recorded by the GNSS antenna. When the dominant wave length exceeds the ship size, the vessel responds coherently to wave forcing, and the distinction between antenna motion and sea surface motion becomes blurred. In this regime, GNSS-IR gradually loses sensitivity to actual wave height, while the vertical motion derived directly from GNSS positioning becomes a more representative indicator of wave energy.

This observation implies that GNSS-IR and GNSS positioning should not be viewed as competing techniques, but rather as complementary components within a unified observation framework. GNSS-IR is best suited for calm to moderate conditions, whereas GNSS-based motion sensing can extend wave monitoring capability into rougher sea states. By integrating these two approaches, it is possible to achieve continuous wave observation across a wider dynamic range of sea conditions than would be achievable using GNSS-IR alone.

Such a hybrid strategy offers a practical pathway for future shipborne wave-monitoring systems, allowing seamless transitions between sensing modes as environmental conditions evolve.

Chapter 5 Conclusions

This study systematically evaluated the performance, limitations, and physical constraints of shipborne GNSS-IR for significant wave height estimation. The results demonstrate that while GNSS-IR is capable of capturing wave-induced sea surface variations under favorable geometric and dynamic conditions, its applicability is inherently limited by satellite availability, observation geometry, and vessel motion effects.

Systematic underestimation of SWH was shown to arise from both modeling assumptions within the LUT and physical interactions between vessel motion and wave dynamics. Although bin-wise correction factors improve agreement with reference measurements, they cannot fully overcome the fundamental limitations imposed by rough sea states.

Future developments in shipborne wave observation should therefore adopt an integrated sensing strategy that combines GNSS-IR with GNSS-based vessel motion analysis. Such an approach acknowledges the physical boundaries of each method and leverages their complementary strengths, offering a robust framework for continuous wave monitoring across a broad range of sea states.

Reference:

Bretschneider, C. L. (1959).

Wave variability and wave spectra for wind-generated gravity waves. Technical Memorandum.

Collins, C. O., Amador, A., Babanin, A. V., & Behrens, J. (2022).

Measuring ocean surface waves: A review of techniques. Journal of Marine Science and Engineering, 10(11), 1661.

https://doi.org/10.3390/jmse10111661

Gulev, S. K., Grigorieva, V. G., Sterl, A., & Woolf, D. K. (2003).

Assessment of the reliability of wave observations from voluntary observing ships. Journal of Geophysical Research: Oceans, 108(C9), 3292.

https://doi.org/10.1029/2002JC001437

Holthuijsen, L. H. (2007).

Waves in oceanic and coastal waters. Cambridge University Press.

Ichikawa, K., Zhu, J. Q., Noda, J., Sakemi, R., Yufu, K., & Matsuura, K. (2024).

Ship-borne wave gauge using GNSS interferometric reflectometry. Coastal Engineering Journal, 66(2), 395–404.

https://doi.org/10.1080/21664250.2024.2342596

idyllicocean. (2018).

New Camellia at Hakata Port in summer [Photograph].

https://idyllicocean.com/vdb/ship18_pic_info.php?p_id=2344

Jin, S., Qian, X., & Kutoglu, H. (2024).

GNSS reflectometry: A new tool and frontiers in Earth observation. Satellite Navigation, 5, 8. https://doi.org/10.1186/s43020-024-00139-4

Larson, K. M., Small, E. E., Gutmann, E. D., Bilich, A. L., Braun, J. J., & Zavorotny, V. U. (2008).

Use of GPS receivers as a soil moisture network for water cycle studies. *Geophysical Research Letters*, 35, L24405.

Ruffini, G., Soulat, F., Caparrini, M., Germain, O., & Martín-Neira, M. (2004).

The Eddy Experiment: GNSS-R speculometry for directional sea-roughness retrieval from low altitude aircraft. *Geophysical Research Letters*, 31.

Sato, Y., & Matsuura, K. (2019).

Forecasting and hindcasting. In *The Naval Architect* (pp. 31–34). Royal Institution of Naval Architects.

https://rina.org.uk/publications/the-naval-architect-archive/

Zavorotny, V. U., & Voronovich, A. G. (2000).

Scattering of GPS signals from the ocean with wind remote sensing application. *IEEE Transactions on Geoscience and Remote Sensing*, 38(2), 951–964.

Acknowledgements

I would like to express my sincere gratitude to my supervisor, Professor Ichikawa, for his continuous guidance, valuable suggestions, and constructive discussions throughout this research. His insights and encouragement greatly contributed to the completion of this thesis.

I am also deeply grateful to Allen Lee and Wei Xinyi for their generous support, technical advice, and many helpful discussions during the development of this study. Without their assistance, this research would not have been possible.

I would like to thank the members of the Ichikawa Laboratory for their helpful comments, discussions, and support during my graduate studies.

Finally, I sincerely appreciate all those who supported and encouraged me during the course of this work.